



Full Length Article

Oxidation kinetics of transition metals exposed to molecular and atomic oxygen

Cristiane R. Stilhano Vilas Boas[#], Jacobus M. Sturm^{*}, Wesley T.E. van den Beld, Fred Bijkerk

Industrial Focus Group XUV Optics, MESA+ Institute for Nanotechnology, University of Twente, Enschede, the Netherlands



ARTICLE INFO

Keywords:

Oxidation
Low Temperature
Transition metals
Electron transport
Atomic oxygen
Molecular oxygen

ABSTRACT

In this work we analyze the oxidation of 30 nm polycrystalline transition metals films (Hf, Ta, Mo and Ru) at low temperatures (298 K to 473 K) upon the exposure to two different species: molecular oxygen and atomic oxygen. Using in-situ spectroscopic ellipsometry and in-vacuum X-ray photoelectron spectroscopy, we verify the oxide growth kinetics and the final stoichiometry after each exposure condition for the four metals, and explore the particularities present in each oxide growth mechanics. The temperature-dependent analysis enabled to experimentally obtain the dissociation energy of molecular oxygen at polycrystalline O covered surfaces. By applying the principles of coupled currents and the Cabrera-Mott oxide growth mechanism, we extract values of the energy barrier for oxidation and the field formed in both oxygen molecule-metal and atom-metal interaction, exploring the differences between both exposure conditions. We demonstrate that in oxide growth at low temperatures two key points should be highlighted: (i) the strong dependence of surface potential on reactive oxygen coverage; (ii) the interrelation between exposure conditions and crystalline oxide formation. The obtained results and analysis contribute to the understanding of oxidation processes at low temperatures, advancing the knowledge required for the design and synthesis of thin metal and oxide films.

1. Introduction

Over the course of materials science development, metal oxidation kinetics have been an extensively studied topic both theoretically [1–6] and experimentally [7–13]. Due to the importance of preventing oxidation for applications such as engineering alloys and bulk metallic structures [14–17], much of these research efforts have focused on high-temperature oxidation and/or exposure at atmospheric pressure. This mostly follows from the fact that, for these applications, changes in the near-surface region (typically observed at low temperature oxidation) do not interfere in components performance. However, the downscaling of devices and consequent growth in metal and metal oxide thin-films use over the past decades has increased the awareness for low temperature oxide growth characterization [12,18–21]. For thin metal films, the growth of a nanometer-thick surface oxide might lead to detrimental changes in properties, such as conductance [22] or reflectivity for extreme UV radiation [23], dramatically altering the performance of a device. On the other hand, controlled oxidation is a valuable asset in the synthesis of thin oxide films. In the field of solid oxide fuel cells, the oxidation states present in the oxide material and at the surface are closely related to its transport properties and surface exchange reactions [24]. For applications such as protective layers against corrosion [25] or as in-

ulating layers in microelectronics [26], changes in the oxide film structure might directly influence the layer properties with respect to oxygen transport. Next to molecular oxygen exposure, metal films may also be exposed to atomic oxygen radical species, either deliberately (as part of an oxide film growth process) or unwanted (e.g. in plasma processes where oxygen containing gases are present as contaminant). In this context, the type of oxygen species to which the metal film is exposed to, might also directly influence the growth rate and final properties of the formed oxide. Therefore, a thorough analysis, bringing mechanistic insights into the stages of molecular- and atomic-oxygen induced oxide growth, covering the differences in oxide composition and structure in the presence of activated oxygen species (such as atomic oxygen) at low temperatures is of great value.

For oxidation at high temperatures and/or formation of thick oxide films, the transport of reactants (oxygen and metal) through the oxide layer is mainly accomplished by thermally activated diffusion. In this regime, the oxide growth process is in most cases well described by the parabolic or the linear rate law [17]. However, this theory is unable to explain the fast growth process observed at low temperatures. The most accepted model for description of low temperature oxidation was initially proposed by Cabrera and Mott [7] and further developed by Fromhold and Cook [27–29], and is usually referred to as the Cabrera-

^{*} Corresponding author.

E-mail address: j.m.sturm@utwente.nl (J.M. Sturm).

[#] Present address: Advanced Research Center for Nanolithography, Science Park 106, 1098 XG Amsterdam, The Netherlands

Mott (CM) model. The main principle of the CM model is based on the significant enhancement of ionic motion by a contact potential, also termed the Mott potential (V_M). This potential is a consequence of the electron transfer from the metal Fermi level to the acceptor levels of adsorbed oxygen species by tunneling or thermionic emission [27,28]. The rise of V_M results in an electric field, which lowers the energy barrier for ionic diffusion through the oxide film, enabling oxide growth. Under the constraint that no net electric charge is transported through the oxide (coupled currents approach [29]), the ion flux is equal to the difference between forward and reverse flux of electrons and this ion current is the rate-determining step of oxidation. For temperatures where the Nernst-Einstein relation ($qV_M \ll k_b T$ – with q the charge of ions, k_b the Boltzmann constant and T the temperature) is not met, the diffusion of ions by the available thermal energy is insignificant compared to the electrical work by the Mott potential. Since the rate of electron transport and field resulting from a constant Mott potential both decrease with increase of oxide thickness, the oxide growth ceases when the so-called limiting oxide thickness is reached.

Even though the CM model is widely employed to describe oxide film formation at low temperatures, the understanding of the factors that influence the formation, magnitude and preservation of the Mott potential – the critical value supporting oxide growth at low temperatures – is still somewhat fragmentary. Cai *et al.* demonstrated the dependence of V_M on pressure and temperature for aluminum exposed to molecular oxygen at temperatures from 223 K to 373 K [30,31]. In another study of Al exposed to O_2 at temperatures between 373 K to 773 K by Jeurgens *et al.* [32], a change of V_M with temperature was not reported. However, the work demonstrated that at $T \geq 673$ K the limiting oxide growth behavior is substituted by a continuous growth of oxide, hypothesized to be related to the transition from a potential-driven to a gradient-driven oxide growth. Lyapin *et al.* have reported a dependency of V_M with pressure for zirconium films exposed to O_2 at 298 K, and a transition similar to Al from potential to gradient-driven oxidation at $T \geq 573$ K [33]. In a complementary theoretical analysis by Sankaranarayanan and Ramanathan [34], it was indicated that the exposure of Zr to atomic oxygen can significantly increase values of V_M compared to molecular-oxygen exposures. These studies provide concrete evidence of the influence of the oxidative environment on potential formation and consequent oxide growth for individual materials. However, to the best of our knowledge, a study that consistently verifies the influence of exposure factors to the formed potential, correlating the oxidation dynamics and driving mechanisms for different metals was not yet performed.

The present study focuses on the analysis of the growth kinetics of a developing oxide and the verification of the final chemical composition and structure of oxide films formed in polycrystalline transition-metal films (Hf, Ta, Mo and Ru) exposed to molecular and atomic oxygen species in a low-temperature range (298 K to 473 K). These metals were selected to include a relatively noble metal (Ru), a metal with high reactivity with oxygen (Hf) and metals with intermediate work functions, since this is expected to influence the formed Mott potential.

The metal thin film deposition (magnetron sputtering), oxygen exposure (atomic and molecular species) and analysis (spectroscopic ellipsometry – SE – and X-ray photoelectron spectroscopy – XPS) were made without break of vacuum and with a transfer time between chambers of less than 15 min, enabling precise characterization of the oxide growth dynamics and final oxidation state without influence of surface contamination. With that, we were able to obtain quantitative information on critical physical processes that determine the oxide growth, such as the molecular oxygen dissociation energy and energy barrier of ionic motion. We verify the influence of exposure conditions (temperature and oxidative specie) on the derived value of the Mott potential, correlating the observed results to the investigated metals properties. We further assess the particularities present for each metal and oxidation condition, and explore the limits of the models adopted for describing the mechanisms that govern the oxide-film growth.

2. Experimental

The experiments were performed in a home-designed ultrahigh-vacuum system with a base pressure of $\leq 1 \times 10^{-9}$ mbar, which allows in-vacuum transfers between deposition (magnetron sputtering), Oxygen Exposure and Analysis Chamber (OEAC) and X-ray spectroscopy (XPS). Reference analysis indicated deposition of less than 1 ML contaminants on metal films left in the system for a 12 h period, confirming negligible surface contamination of samples during the experiments. The OEAC is equipped with an SE (Woollam M-2000), a Specs MPS-ECR mini plasma source and an annealing stage. Films of 30 nm Hf, Ta, Mo and Ru were deposited onto substrates of thermally oxidized Si(100) (300 nm SiO_2 on Si, grown by dry oxidation at 1373 K) by DC magnetron sputtering at room temperature, using Ar as working gas with a deposition pressure of 5×10^{-4} mbar and growth rate of typically 0.05 nm/s. Oxide layers were grown at the OEAC as a function of exposure time (t) by heating the vacuum transferred samples to temperatures (T) of 298 K, 323 K, 373 K, 423 K or 473 K (± 5 K), and subsequent exposure to pure (99.999 vol%) molecular or neutral atomic oxygen at a partial pressure (p_{O_2}) of 1×10^{-4} mbar. Each exposure condition (combination of metal, oxidative specie and temperature) was applied to a freshly deposited metal film. The atomic species (which have thermal energy) were generated by a Specs MPS-ECR mini plasma source, with atomic oxygen flux in the order of 10^{15} atoms/cm²/s. For the exposures, the sample was placed directly below the oxygen source, guaranteeing a homogeneous flow of species to the surface.

The evolution of oxide thickness was monitored by in-situ SE at an angle of incidence of 75° and a spectral range of 245.8–1688.1 nm. The oxide thickness was determined by a multi-layered model developed in CompleteEASE® software (Developed by J. A. Woollam Co., Ltd). The procedure for model development is detailed in Section 2.1. After the end of exposure and cooling of the films, the grown oxides were in-vacuum transferred to a Thermo Theta Probe X-ray spectrometer, from which angle-resolved XPS (AR-XPS) measurements were acquired. The measurements were performed with monochromatic Al-K α (1486 eV) radiation and 400 μ m spot size, aligned at the center of the sample. The collection and analysis of data was made by the use of Avantage software. The background of the spectra was subtracted according to Shirley model, and peak fitting was performed with a product of Gaussian and Lorentzian shapes. Quantification was based on Scofield sensitivity factors [35] and a model of uniform elemental distribution. Fits to XPS data were performed by first evaluating the spectra of as-deposited metals (also deposited and vacuum-transferred to XPS), in order to assess the metal peak position and asymmetry. The metal peak positions were fixed to the reference measurements for comparison of oxide composition between samples. Oxide peaks in the metal core levels of oxygen exposed samples were fit with a symmetric peak for oxides of Ta, Mo and Hf, an asymmetric peak for oxides of Ru [21,36,37]. Molybdenum and tantalum might exhibit multiple oxides with different stoichiometry within a small binding energy range [21,36]. Therefore, when applicable, these oxide components were fit with a single peak with varying full width at half maximum (FWHM), and a larger FWHM was interpreted as a metal containing stoichiometric and non-stoichiometric states [21]. This approach to assess possible presence of non-stoichiometric states from the peak shape, rather than from the ratio of the O1s to metal core peak area, was motivated by observations in our lab and from previous reports [38] that slight reduction of metal oxides (e.g. by electron or radiation induced reduction) is more readily observed from the metal core level peak shape than from the O vs. metal peak area. Additionally, this approach avoids systematic uncertainties due to sensitivity factor and electron analyzer transmission.

The metals and grown oxides structures were verified by ex-situ X-ray diffraction (XRD), performed with a PANalytical Empyrean X-ray diffractometer (Cu-K α radiation, 0.154 nm), using in-plane grazing incidence XRD (GIXRD) geometry at a fixed incident angle (above the critical angle). The same diffractometer was used in X-ray reflectometry

(XRR) mode for determination of reference metal and oxides thicknesses applied in the development of ellipsometry models.

2.1. Ellipsometry model development

For the analysis presented in this paper, the model development consisted of a multi-step approach with support characterization techniques to minimize the number of variables during the fitting. The base for the model consisted of characterization of single layers of metal and stoichiometric oxide. The stoichiometric oxides were obtained by reactive direct current (DC) magnetron sputtering of the respective metallic target with a mixture of oxygen and argon. Three different thicknesses of these layers were deposited on SiO₂/Si substrates and evaluated in-situ by ellipsometry and ex-situ by X-Ray reflectivity (immediately after removing from vacuum). The values of thickness obtained via XRR were used as input parameters in the ellipsometric model, and optical constants for each material were determined. For the substrate, an existing model (JAW for thermally oxidized Si) was applied. For oxide layers, a Cauchy-type function was used to describe the refractive index n while the extinction coefficient k was set to zero over the entire concerned wavelength range (for Hf oxide) or above UV range (for oxides of Ru, Ta and Mo) [39]. For the standard Cauchy layer, the software assumes an exponential decay shape for the k function. For metals, a B-spline model was applied, using the parameters from the software database as a starting reference. To guarantee a realistic model for the grown oxide film and overcome possible data misinterpretation induced by substoichiometric components, an extra layer of substoichiometric oxide was added between the stoichiometric oxide and the metal. The placement of this layer was based on AR-XPS analysis (see section 3.2). This extra layer was modeled by the effective-medium approach (EMA) using Maxwell-Garnett formulation, with the modeled stoichiometric oxide as matrix and modeled metal as “void” material [40]. It should be noted that this approach does not necessarily provide a proper description of the optical properties of substoichiometric oxide, but serves as first order approximation. Finally, these single layer models were combined for the fitting of oxide layers grown on metals. For all measurements, the substrate and pristine metal layer were evaluated before oxygen exposure, increasing the reliability in fitting of the multi-layered model.

3. Results and discussion

3.1. Oxide growth kinetics by ellipsometry

We begin our analysis by focusing on the general evolution of oxide growth as a function of oxidation time for Hf, Mo, Ta and Ru under exposure to molecular or atomic oxygen, presented in Figure 1 a-h. It is important to observe the difference in the vertical scale – oxide thickness – between figures. The analyzed temperatures are far below temperatures in which the formation of volatile oxides is expected (e.g. volatile MoO₃ is reported above 675 K [41] and other oxides are expected to have better temperature stability). Therefore, changes in ellipsometry signal were related to the growth of a top oxide layer. The oxide thickness data was extracted by fitting obtained in-situ SE spectra following the procedure described in Section 2.1, with the plotted values corresponding to the sum of the two modelled oxide layers (stoichiometric and substoichiometric). A general trend of growth is shared among all metals, where it is interesting to note that some peculiarities are present for each combination of metal and oxidative specie.

According to the CM theory, at low temperatures, the oxide growth is expected to be initiated by a fast formation of a closed oxide layer (first phase of oxide growth). The formation of a stable film allows a voltage (V_M) to build up across the oxide, and consequent growth of oxide by a field-induced mechanism (second phase). With increasing oxide thickness the field will become too weak to assist diffusion and the oxide growth ceases [7,29].

It is reasonable to assume that a monolayer of oxide has an average thickness of 0.3 nm [42]. As Mo exposed to O₂ at $T \leq 373$ K and Ru exposed to O₂ at $T = 323$ K show a maximum oxide thickness equal to or less than about 1 monolayer of oxide, we can conclude that the oxide formation under these conditions is restricted to the first phase of oxide growth, and therefore no CM field is generated.

The limiting oxide is considered to be reached when the oxide growth rate has reduced to about one “oxide” monolayer per 10⁵ s ($\sim 10^{-15}$ m/s) [7,32]. According to this rule, we observe a self-limiting behavior of oxide film growth for: Hf from 298 K to 423 K for both species; Ta from 298 K to 423 K for O₂, and from 298 K to 373 K for O; Mo from 298 K to 323 K for O; Ru from 298 K to 473 K for O₂, and from 298 K to 423 K for O. For most of these cases, an increase in temperature leads to a higher oxide growth rate and larger limiting oxide thickness. However, for Ru exposed to O₂, as mentioned, a considerable decrease in limiting oxide thickness with the increase of temperature from 298 K to 323 K is observed. For $T > 323$ K, the increase in thickness and rate with increase of temperature is restored.

For the exposure conditions that do not present a self-limiting oxide growth (Hf at 473 K for both O and O₂; Ta at 473 K for O₂, and from 423 K to 473 K for O; Mo at 473 K for O₂, and from 373 K to 473 K for O; Ru at 473 K for O) there are also differences among its oxidation behavior. Hf, Ta and Mo exposed to O₂ and Ru exposed to O at 473 K show a rapid initial oxide growth, followed by a decrease in rate with increasing exposure time. However, this second oxidation stage is continuous, and a transition towards a limiting oxide thickness is not observed. For Ta and Mo exposed to atomic oxygen at $T \geq 423$ K, the initial rate is slower than that obtained for lower temperatures. In these exposure systems, an almost linear oxide growth is set, and a saturating growth of oxide thickness is not observed. On the other hand, Hf exposed to O at $T = 473$ K presents a significantly higher growth rate during the entire oxidation process, reaching a much thicker oxide compared to the other metals after 300 min exposure.

3.2. Analysis of final oxide composition and structure

We now follow the analysis by individually assessing the composition of the formed oxides. Figure 2 shows in-vacuum XPS analysis for example cases of samples exposed to atomic oxygen at 473 K and a take-off angle of 34.25° (highest probing depth available). The data of the remaining exposure conditions, a representative more surface sensitive probing angle and reference metal samples are presented in the Supplementary Materials.

Except for the final oxide thickness, Hf films exposed to molecular and atomic oxygen present similar composition evolution as a function of temperature. As seen in Figure S.1 and described in Table S.1, Hf exposed to both species at $T \leq 373$ K shows Hf 4f_{7/2} (HfO₂) peaks centered at energies slightly lower than 18.3 eV, the energy characteristic of stoichiometric HfO₂ [37,43]. This can be interpreted as a slightly lower stoichiometry, as the increase in metal content leads to a shift of oxide peaks to lower energies. However, for the same samples, the higher angles of AR-XPS analysis (i.e. depth information more limited to the surface) show the formation of a stoichiometric oxide closer to the surface. This indicates metal interstitials or oxygen vacancies as the dominant migrating species in oxide formation [18,40]. The increase of temperature to 423 K and 473 K leads to the formation of homogeneously stoichiometric oxides from the surface up to the maximum analysis depth of XPS, with peaks centered at 18.3 eV.

Tantalum can be found in multiple oxidation states (Ta²⁺, Ta⁴⁺, Ta⁵⁺) [36], with the most stable, stoichiometric form (Ta⁵⁺) presenting a binding energy of 26.6 eV. Ta exposed to molecular oxygen up to 373 K shows oxide peaks centered at 26.6 eV of low intensity and high FWHM. Considering the small thickness of these oxide overlayers, the high FWHM can be related to a larger spread in binding energies due to a relatively high contribution from different binding energies at the surface and interface of the oxide layer. As in the case of Hf, AR-

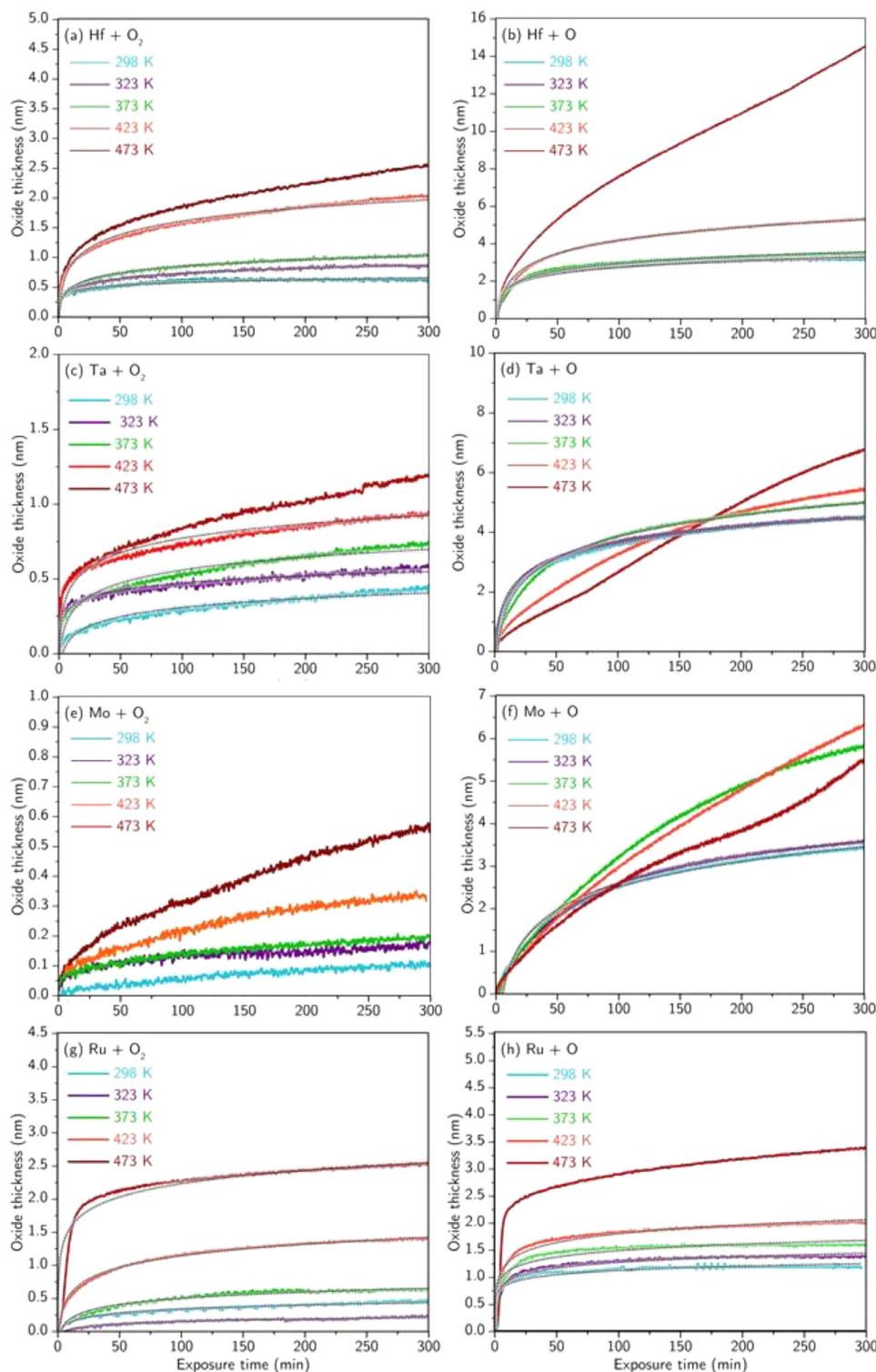


Fig. 1. Oxide thickness extracted from in-situ SE of metals exposed to molecular or atomic oxygen at different temperatures. a) Hf + O₂ b) Hf + O; c) Ta + O₂, d) Ta + O; e) Mo + O₂, f) Mo + O; g) Ru + O₂, h) Ru + O. The fitted black dashed lines correspond to the theoretical growth curves based on the Cabrera-Mott inverse logarithm law (Eq. 6). The shadowed area along the fits corresponds to the fitting error.

XPS reveals a higher stoichiometry at depths closer to the surface, with an increase of intensity and decrease of FWHM for oxide peaks. The increase of exposure temperature to 423 K reduces the FWHM and leads to a slight peak shift to lower binding energy (Table S.2), which is maintained throughout all analysis angles. This indicates that the increase of temperature leads to a change in oxide stoichiometry. On the other hand, all atomic-oxygen exposed samples present a constant FWHM (1.1 eV) and peak centered at ~ 26.6 eV from surface to maximum probed depth. Therefore, we can conclude that for atomic-oxygen exposed tan-

talum, a stoichiometric oxide film is formed independently of the applied temperature.

As previously mentioned, molybdenum can also form oxides of multiple stoichiometries, with Mo⁴⁺ (229.5 eV) and Mo⁶⁺ (232.3 eV) the most stable forms [21]. The XPS spectra of samples exposed to molecular oxygen show virtually no oxide peaks up to 353 K. However, O1s peaks at energies corresponding to metal oxide compounds (529 – 531 eV) are observed (Figure S.6). This is in agreement with the results obtained by in-situ SE, which indicate for these samples the formation of

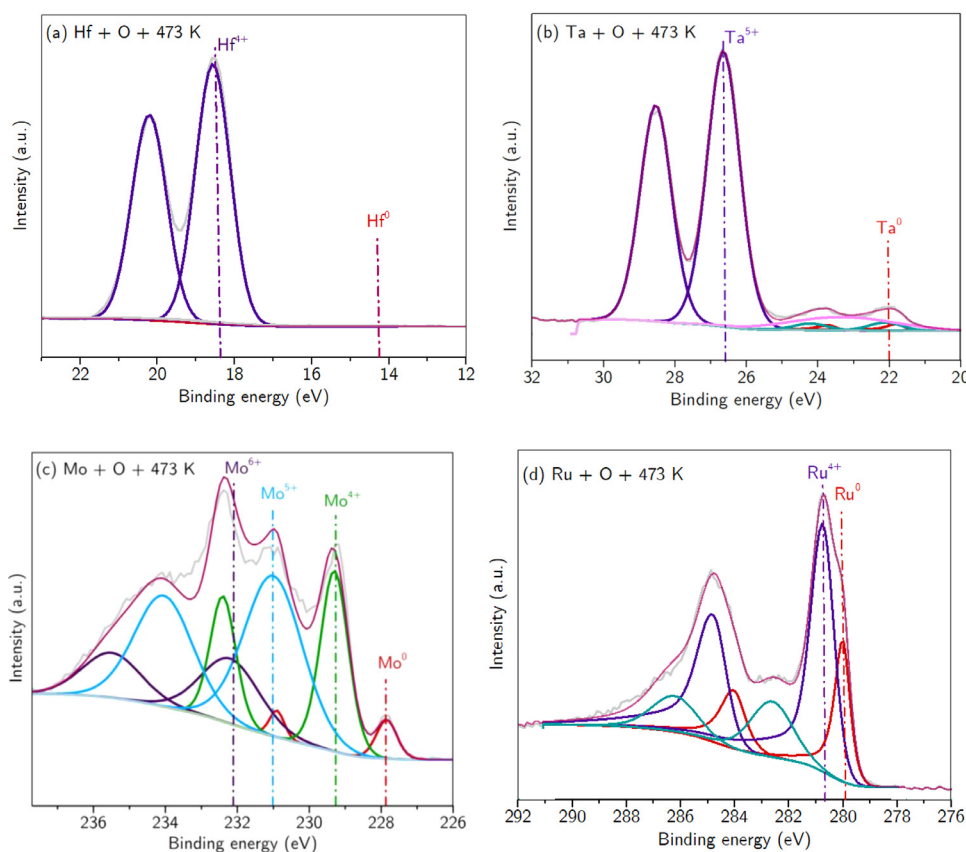


Fig. 2. XPS measurement of metals exposed during 300 min to atomic oxygen at 473 K and a take-off angle of 34.25°. The light grey line indicates measured data, colored lines indicate fitted peaks for the specified chemical state. The pink line represents the sum of background and fitted components. a) Hf; b) Ta (the broad light pink peak at ~23 eV corresponds to O 2s); c) Mo; d) Ru (the light blue peaks at ~282.5 eV correspond to intrinsic plasmon features).

an oxide with thickness of less than 0.15 nm. For O₂ exposed samples at 423 K and 473 K, low intensity Mo⁴⁺ peaks are observed, which correspond to the formation of a thin MoO₂ layer. From 298 K to 423 K, the atomic-oxygen exposed samples present a broad peak, centered at about 232.3 eV, indicating the formation of MoO₃ as dominant stoichiometry. For these samples, AR-XPS indicates a slightly lower FWHM near the surface (Table S.3). Contrary to Hf and Ta, the FWHM then increases with temperature, implying an increase of stoichiometry distribution for higher temperatures. At 473 K, the stoichiometry distribution is so evident that peaks relative to different oxidative states can be easily distinguished in the spectrum, which is kept throughout the oxide depth. For this sample, the most prominent peak corresponds to a well-defined peak at 231.1 eV, which is associated to the less stable Mo⁵⁺ state.

Ru is a well-known oxidation-resistant material at ambient conditions [23,44]. The small shift between Ru⁰ (280 eV) and Ru⁴⁺ (280.7 eV) can sometimes interfere in the identification of substoichiometric forms, due to the overlap between peaks from substoichiometric oxide and metal. However, the comparison between metallic Ru (Figure S.7d) and Ru exposed to O₂ at 298 K, indicates a more pronounced shoulder on the high binding energy side of both peaks for the exposed sample, suggesting the presence of oxidized Ru (peak centered at ~280.4 eV). On the other hand, the spectrum for O₂ exposure at 323 K presents really sharp Ru 3d core levels peaks. This suggests that, as also observed by in-situ SE, virtually no oxide is formed at the surface. The increase of temperature then leads to more pronounced RuO₂ peaks centered at ~280.7 eV, indicating compositions close to stoichiometric for these exposure conditions. For atomic oxygen exposures, the RuO₂ features are clearly seen for all samples, and an intensity increase and a shift to higher binding energies with increase of temperature is observed (Table S.4). Since Ru and the RuO₂ overlayer are conducting, both have intrinsic plasmon losses contributing to the signal in the spectral range close to the Ru 3d core level [45]. These features are seen at ~282.5 eV for thicker oxides (O₂ exposed at $T \geq 423$ K and O exposed at $T \geq 323$ K).

Following the in-vacuum analysis, analysis of the crystalline structure of pristine and oxidized metals was made by ex-situ GIXRD. To minimize influence of atmospheric exposure and further oxide growth, the samples were analyzed immediately after being removed from vacuum.

For as-deposited metals, the Scherrer equation [46] was applied for estimating the in-plane diameter of the crystallites. The values obtained lie between 15 and 20 nm and, as typically observed for polycrystalline thin films, the grain size perpendicular to the plane of the film is expected to be similar to the film thickness [47]. In our analysis, no angular dependence of the diffracted intensity was observed apart from that induced by the illumination geometry, which suggests a random orientation of crystallites [48]. With atomic force microscopy (AFM) (not shown), root mean square roughness values of 0.2 to 0.3 nm were determined for the as-deposited films, indicating similar initial surface and structural conditions for consequent oxidation of films. To verify a possible influence of increased temperatures on metal atomic arrangement, AFM and GIXRD for samples prior and after annealing at 473 K in vacuum were compared. These analyses indicated no influence of the applied temperatures on the metal structure (as expected due to the low values of applied temperatures relative to the melting temperature of each metal).

Figure 3 shows examples of GIXRD spectra of key cases. It was observed that only Hf, Ta and Mo exposed to atomic oxygen at 473 K formed crystalline oxides, as highlighted by the appearance of characteristic monoclinic HfO₂ [49] and orthorhombic Ta₂O₅ [50] and MoO₃ [51] peaks in the spectra. The remaining experiments resulted in an amorphous oxide. All of the amorphous oxide films had final thickness equal to or lower than about 6 nm. It is remarkable to note, however, that even though Mo exposed to atomic O at 423 K and 473 K present similar growth dynamics and final oxide thickness, only the sample exposed to the higher temperature shows the formation of crystalline oxide. Furthermore, one should note that even though the XPS spectrum

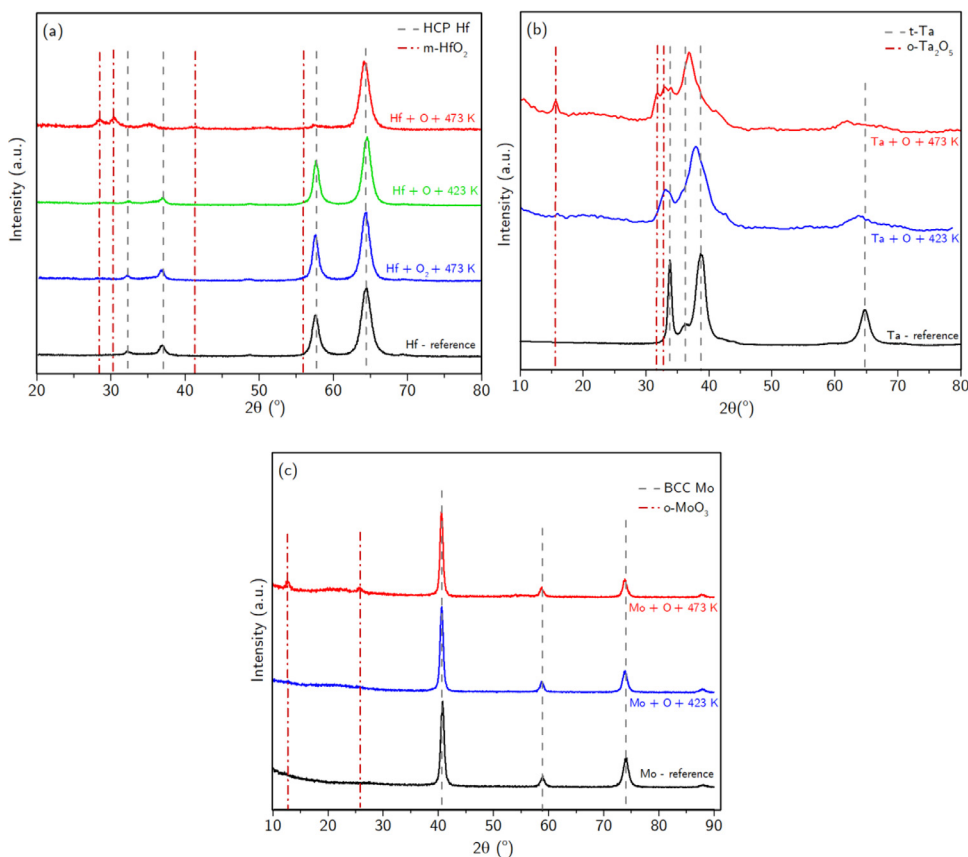


Fig. 3. GIXRD analysis of a) Hf, b) Ta and c) Mo exposed to different conditions. The dashed grey lines represent characteristic peak positions of crystalline metal (HCP Hf, tetragonal Ta and BCC Mo) and dashed-dot dark red lines characteristic peak positions of crystalline oxides (monoclinic HfO₂, orthorhombic Ta₂O₅ and MoO₃).

of Figure 2c indicates a dominant Mo₂O₅ contribution, the GIXRD analysis of the same sample shows the characteristic peaks related to MoO₃. Considering the lower stability of Mo⁵⁺ state, the air exposure prior to XRD analysis might have induced the transition of Mo₂O₅ to MoO₃.

To facilitate an overview of all observed scenarios, Table 1 brings a summary of the main characteristics observed for the analyzed exposure systems. In the following sections, we will explore the entire process of oxide formation, correlating the obtained data and calculated parameters to properties of the studied metals.

3.3. First step of oxidation: molecular oxygen dissociation and surface-limited growth

We can use the advantage of real time SE monitoring to obtain more information about the very initial stages of oxide formation. For molecular-oxygen exposure, the oxidation begins by the dissociation of molecules and atomic oxygen binding to surface atoms (dissociative chemisorption) [29,52]. For molecular oxygen on transition-metal surfaces, two different pathways can be followed: trapping-mediated and direct chemisorption. The trapping-mediated mechanism involves a two-step process [53]. The first step is the non-activated formation of a stable, molecular precursor, as stated in Eq. (1):

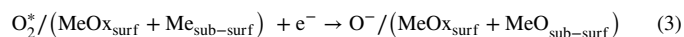


where O₂^{*} represents a precursor with a stretched oxygen bond compared to a free molecule and Me the metal surface. Once trapped at the metal surface, the precursor can either desorb into the gas phase or proceed to chemisorb dissociatively, with the relative rates dictated by a surface temperature mediated kinetic competition [54–56]. If not desorbed, the second step is the activated transition of the precursor to the chemisorbed atomic oxygen state when the O-O bond is disrupted, and the O atoms approach closer to the metal surface [53]:



In the direct mechanism, the molecule proceeds directly to the process described by Eq. (2), with no formation of intermediate precursors.

However, we should emphasize that at the applied oxygen pressure, the time needed for saturation of the metal surfaces with dissociatively chemisorbed oxygen atoms is expected to be much faster than the time resolution of the applied ellipsometry measurements (2.48 s acquisition step). Previous studies have shown that the saturation of the O coverage on Ta surfaces occurs upon exposure to 10 L of O₂ [57]. Preliminary studies made in our research group have demonstrated the saturation of surface O coverage on a Ru surface with about 100 L of molecular oxygen. Based on the applied oxygen flux, we estimate that the metal surface should already be saturated within approximately 1 s of O₂ exposure. Therefore, we propose that the initial oxide growth rate as monitored by ellipsometry corresponds to the dissociation of molecular species on an oxygen saturated surface in conjunction with incorporation of oxygen atoms in sub-surface layers, following a mechanism represented by Eq. (3):



As previously mentioned, we assume the oxide monolayer to have a thickness of less than 0.3 nm, after which the limiting step of oxide formation might be substituted by the diffusion of ions through the formed oxide. In cases where the molecular dissociation of O₂ on an oxygen saturated surface acts as the limiting step for the initial phase of oxide formation, we propose that the energy barrier for this process can be derived from an Arrhenius analysis. With that, we can write a relation only for this initial oxide growth formation as described in Eq. (4):

$$\frac{dx}{dt} \Big|_{x < 0.3 \text{ nm}} = A \exp\left(-\frac{E_a}{k_b T}\right) \quad (4)$$

with E_a the dissociation barrier of molecular oxygen and A a pre-exponential factor. Taking the natural logarithm of Eq. (4), we obtain a

linear relation between the initial rate and the inverse of temperature:

$$\ln\left(\frac{dx}{dt}\bigg|_{x<0.3\text{nm}}\right) = \ln(A) - \frac{E_a}{k_b}\left(\frac{1}{T}\right) \quad (5)$$

Hence, by plotting the logarithm of the initial rate of oxide growth as a function of $1/T$ for the oxidation, we can determine the activation energy needed for molecular oxygen dissociation at the analyzed surfaces.

Now we should evaluate for which set of exposure conditions this analysis is valid. Naturally, the metals should have been exposed to molecular oxygen. Furthermore, the processes involved in dissociation should be limiting and should not change along the analyzed temperature range. Hf and Ta do not show evidences of different processes acting on the initial stages of oxidation, as there is a clear oxide formation with rates scaling with temperature. However, the cases of Ru and Mo deserve each a more detailed discussion.

For Mo it is known that a low oxygen uptake and oxide growth is given upon thermal oxidation at low temperatures [58–61]. Previous studies have shown that such behavior is related to a sharp decrease in surface reactivity of the initially formed thin MoO_2 towards oxygen species [60]. However, before the formation of the first oxide monolayer, earlier studies on monocrystalline Mo surface have shown a similar dissociation and oxidative behavior from room temperature up to about 573 K [59], indicating that the same dissociation mechanism might act in this temperature range. As our analysis was performed at temperatures below this range, we can assume a constant dissociation mechanism to be present and, therefore, the developed analysis can be applied to the performed exposure conditions.

For Ru, as previously mentioned, with the increase of temperature from 298 K to 323 K a decrease in limiting oxide thickness is observed. This can be attributed to a decrease in equilibrium oxygen coverage at 323 K (compared to 298 K), as also previously reported by Cai *et al.* for Al exposed to O_2 at temperatures ranging from 223 K to 373 K [30]. Similarly, a lower initial oxidation rate is observed with increase of temperature from 298 K to 323 K, which is also attributed to oxygen coverage being the limiting factor for oxide growth. Wheeler *et al.* [54] have demonstrated the existence of a trapping-mediated mechanism on the O_2 -Ru reaction for molecules with low incident energy. In this study, an inverse dependence of the initial dissociative chemisorption probability with surface temperature was observed, related to the kinetic competition between oxygen desorption and dissociation at the Ru surface (a similar mechanism was also observed for Al surfaces by Hofmann *et al.* [62]). For Ru at T above 323 K, two possibilities are raised: i) the temperature-induced dissociation becomes more prominent than desorption, therefore the availability of oxygen is no longer a limiting factor; or ii) the mechanism changes from trapping-mediated to direct chemisorption [54,55]. Therefore, for Ru at $T \leq 323$ K, the limiting step for oxide formation will not be the oxygen dissociation itself, but the kinetic competition between oxygen desorption and dissociation; and/or there is a change in the predominant dissociative chemisorption mechanism. In either case, to guarantee that the analyzed temperature range is undergoing the same surface processes, it is reasonable to include only the exposures of Ru to O_2 at temperatures above 323 K in the proposed oxygen-dissociation analysis.

The conditions assumed to be consistent with the proposed analysis were then evaluated and the logarithm of the initial rate of oxide growth as a function of $1/T$ is plotted in Figure 4. Indeed a linear relationship between the terms is observed for all metals. The extracted values of the energy needed for molecular oxygen dissociation (E_a) in each metal surface obtained from this analysis are shown in Table 2.

A small difference in dissociation barrier of molecular oxygen was found compared to typical differences obtained for theoretically calculated dissociation energies of O_2 on different clean metals (cf. refs 53 and 55, it should be noted that theoretical calculations with similar methodology were not found for most of the metals studied in this work). This suggests that the effective energy barrier for dissociation of O_2 on a metal surface saturated with oxygen, in conjunction with the migration

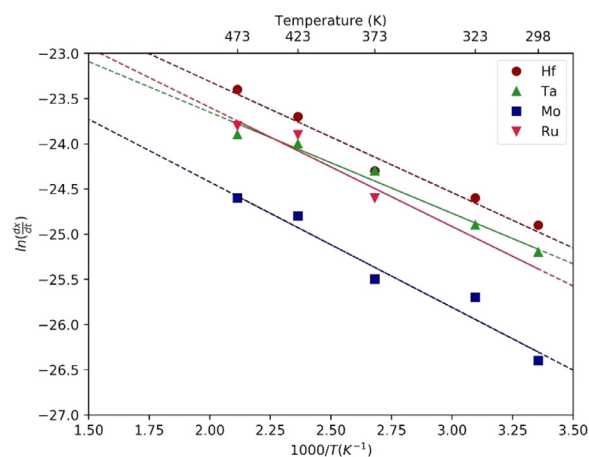


Fig. 4. Natural logarithm of the initial oxide growth rate for exposure to molecular oxygen as a function of the reciprocal of temperature for all analyzed metals. Only data for temperatures for which thermally activated dissociation of molecular oxygen is the limiting factor for oxide growth are included.

of oxygen to the sub-surface layer is less strongly dependent on reactivity of the metal. Unfortunately, to our knowledge there is little theoretical background on expected activation energies for this stage of oxidation. However, a certain order of the calculated values ($\text{Hf} < \text{Ta} < \text{Mo} < \text{Ru}$) is still observed. It is known from literature that the oxygen adsorption, dissociation and formation of a chemical bond with the metal surface is a consequence of the electron donation from the metal surface into the antibonding orbitals of the oxygen molecule [55]. Looking at transition metals, the d-band filling increases and d-band center becomes lower in energy and large in spatial extent in the direction from the top-left to the lower-right end of the periodic table, which results in a weaker covalent interaction and strong Pauli repulsion between metal surface and oxygen [63,64]. Therefore, it is expected that the interaction with oxygen (and other adsorbents) should follow an order similar to that observed with our calculations. To the best of our knowledge, no previous quantitative analysis of molecular oxygen dissociation was performed for initially polycrystalline metallic surfaces as the ones analyzed in our experiments, at least after saturation of the surface with oxygen. However, a comparison with simulation [53,64] and experimental data on single crystalline metals [63] support the observed trends and differences in dissociation energy.

3.4. Second step of oxidation: oxide growth beyond few monolayers

Following the analysis of initial oxide formation, we now focus on the dynamics of oxide growth after the formation of the first oxide layer. As previously mentioned, the main mechanism driving low-temperature oxidation is reported to be the electric-field-driven, described by CM theory. However, a change in exposure conditions can interfere in the main parameters determining oxide growth and formed oxide properties. In the following sections, the predominant mechanism for each exposure condition was evaluated. A calculation of main parameters describing oxide growth kinetics, together with a correlation between the obtained results and exposure conditions (the combination of temperature, oxidative specie and metal of interest) was performed.

3.4.1. Limiting oxide growth and the influence of coverage on V_M

As previously mentioned, the self-limiting behavior of oxide film growth observed for Hf (298 K to 423 K for both species), Ta (298 K to 423 K for O_2 and 298 K to 373 K for O), Mo (298 K to 323 K for O) and Ru (298 K to 473 K for O_2 , 298 K to 423 K for O) is consistent with the Cabrera-Mott model of electric-field-driven oxide growth [7,32]. According to CM, with the establishment of V_M , the growth rate of oxide

Table 1.
Summary of characteristics from oxide growth dynamics and final formed oxide on metals exposed to O₂ and O.

Oxide characteristic	O ₂ exposure	O exposure
Hf	Limiting oxide formation	CM growth for $T \leq 423$ K
	Stoichiometry	Stoichiometric at all T
	Structure	Amorphous for all T
Ta	Limiting oxide formation	CM growth for $T \leq 423$ K
	Stoichiometry	Lower stoichiometry at $T \leq 373$ K
	Structure	Amorphous for all T
Mo	Limiting oxide formation	Does not follow CM ($T \leq 423$ K surface-limited; $T = 473$ K: continuous growth)
	Stoichiometry	Substoichiometric when formed
	Structure	Amorphous when formed
Ru	Limiting oxide formation	CM-type growth for 298 K, 353 K $\leq T \leq 423$ K
	Stoichiometry	Lower stoichiometry at $T \leq 373$ K
	Structure	Amorphous for all T

Table 2.
Effective O₂ dissociation barrier for initial oxide growth (< 0.3 nm) for the analyzed polycrystalline metals.

	E_a (eV)
Hf	0.100 ± 0.004
Ta	0.110 ± 0.002
Mo	0.120 ± 0.005
Ru	0.130 ± 0.006

thickness x follows the equation:

$$\frac{dx}{dt} = \Omega n \nu \exp\left(\frac{-U + q a V_M/x(t)}{k_b T}\right) \quad (6)$$

where Ω is the volume of oxide formed per cation, n is the number of cations per unit area which may jump through the rate-limiting energy barrier U , ν is the attempt frequency of the cation, q is the charge of the migrating cation, $2a$ is the distance between potential minima. The field that decreases the energy barrier for ionic diffusion is re-written as the term $V_M/x(t)$, highlighting its dependence on oxide film thickness. In our previous study on low-temperature oxidation [11], we have demonstrated that the reaction front of oxide formation in the analyzed transition metals corresponds to the oxygen/oxide interface. This was further confirmed by the AR-XPS analysis performed in this study, which showed that for the cases that follow CM-type growth, a higher stoichiometry is found near the surface. This higher stoichiometry near the surface is characteristic of reactions where metal interstitials (M_i^{z+}) or oxygen vacancies (V_O^{z+}) are the dominant migrating species.

Therefore, for the mentioned conditions and with known values of Ω , n , ν , q and a , parameters V_M and U can be obtained by fitting the inverse logarithm law given by Eq. (6) to the growth rate curves shown in Figure 1 [29,30,65]. The fitting results are shown as black dashed lines in Figure 1. As checked by GIXRD analysis, for the cited cases which follow a CM-type growth, the oxidation results in an amorphous oxide growing on a polycrystalline metal. Therefore, we assume an isotropic diffusion in the oxide film, with the rate-limiting barrier for cation motion located within the oxide. From this assumption, n and a are estimated based on the hopping of metal cations between interstices of the corresponding oxide. Considering their amorphous nature, the values for Ω , n and a were obtained based on bulk values of density and molar mass of the oxides. For the calculations performed in this paper, $\nu = 10^{12}$ s⁻¹ [7] and $q = ze$ C (with the elementary charge $e = 1.6022 \times 10^{-19}$ C, and $z = 4$ for Ru and Hf, $z = 5$ for Ta and $z = 6$ for Mo). All the applied values for Ω , n , ν and $2a$ are shown in Table 3, together with values of U obtained from the fittings for both, molecular- and atomic-oxygen exposures. The values of V_M are shown in Figure 5 as a function of exposure temperature for both species.

From the performed analysis, we noted the activation energy barrier to be independent of T and present similar values for metals exposed to molecular and atomic oxygen. This supports the obtained fitting results,

Table 3.

Fitted values for the rate-limiting energy barrier for cation motion (U), for dry thermal oxidation of metals under exposure to atomic and molecular oxygen at $pO_2 = 1 \times 10^{-4}$ mbar. The values of V_M are displayed in Figure 5 as a function of temperature. The corresponding constants applied for the volume of oxide formed per cation (Ω), number of cations per unit area (n), and distance between potential minima ($2a$) are also displayed. These were estimated based on bulk values of density and molar mass of the oxides and assuming the rate-limiting barrier for cation motion to be located in the oxide film.

Metal	Oxidative specie	Ω (nm ³)	n (nm ⁻²)	$2a$ (nm)	U (eV) (fitted)
Hf	O ₂	0.108	9.1	0.23	1.5 ± 0.2
	O				1.8 ± 0.3
Ta	O ₂	0.313	7.9	0.23	1.8 ± 0.2
	O				1.9 ± 0.3
Mo	O	0.204	7.3	0.23	1.7 ± 0.1
Ru	O ₂	0.095	9.9	0.22	1.8 ± 0.4
	O				2.0 ± 0.3

as the activation energy for oxidation is related to the energy necessary for the ions to diffuse through the formed oxide and thus should be independent of oxidation conditions as long as in depth transport is rate limiting [32]. As in both molecular- and atomic-oxygen exposures amorphous oxides were formed, U values should not be dramatically different. This also suggests a similar atomic structure in the formed amorphous oxide films among the analyzed temperatures. On the other hand, the V_M formed across a metal oxide changed dramatically between molecular- and atomic-oxygen exposure, presenting also a slight variation with temperature, as seen in Figure 5.

We shall initially focus on the effect of temperature on potential for each oxidative specie. As seen in Figure 5a, for O₂ exposure the increase of T does not significantly affect V_M of Hf and Ta, only values for Ru are influenced. As discussed in Section 3.3, this variation seen in Ru might be due to enhanced desorption upon increase of T and thereby reduction of oxygen coverage. One should note that, as a closed oxide layer was probably not formed for 323 K, the data point might not represent a real value of V_M . However, it serves as an indication of the effect of coverage on the formed potential, indicating that at temperatures where dissociative chemisorption becomes again more prominent than desorption ($T \geq 373$ K), values of V_M are restored.

For direct atomic oxygen exposure, the change in temperature is critical only for Ta. It is important to observe that also for Ta, the increase in T induces a decrease in growth rate at the initial fast oxidation stage. Based on the analysis developed by Jeurgens *et al.* on Al oxidation [32], a decrease of the rate in the fast oxide growth stage and a reduction of V_M can be related to either of the following phenomena: (a) increase of oxygen desorption (reduction of coverage) or (b) low rate supply of oxygen (due to low exposure pressure). For our experimental conditions, the atomic oxygen supply is in the order of 1 ML/s, making it improbable that the supply is the limiting factor for oxide growth. Furthermore, when exposing Ta to molecular oxygen, no effect

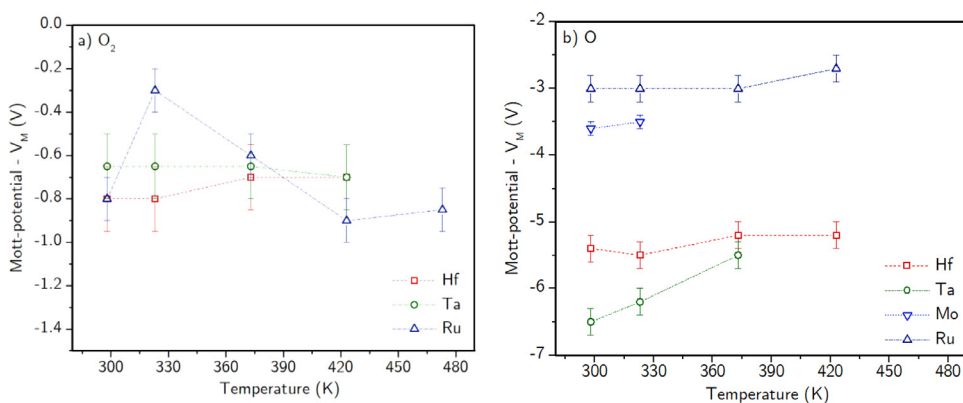


Fig. 5. Calculated Mott potential (V_M) as a function of temperature for each metal-oxidative specie combination. a) Metals exposed to O_2 , b) metals exposed to O. The corresponding constants applied for the volume of oxide formed per cation (Ω), number of cations per unit area (n), and distance between potential minima ($2a$) are displayed in Table 3. The dotted lines serve as guides to the eyes.

evidenced the increase of desorption with the increase of temperature. As atomic-oxygen presents an even higher sticking probability than O_2 [63], it is also unlikely that temperature induced desorption of atomic oxygen might increase in the analyzed temperature range. However, the increase of temperature might lead to an increased ionic diffusion, such that thermal diffusion induced by concentration gradients becomes significant compared to field assisted (self-limiting) oxide growth. This higher diffusion leads to a rapid consumption of adsorbed O and consequent reduction of atomic oxygen coverage. With that, according to the coupled currents approach, the potential starts to shift to the so-called “kinetic” potential V_K , which is lower than the Mott potential V_M [27–29,32]. Therefore, we propose that the increased influence of the thermal diffusion leads to the observed growth behavior, resulting in the decrease of initial oxide growth rate and surface potential.

Following this analysis, we can now discuss the difference in V_M between oxidative species for all metal cases. As O_2 is an (electron) acceptor, electrons from the metal are transferred to the molecule upon contact with the metal surface [29,63]. This process leads to the dissociation of molecular oxygen (following the energy trend calculated in Section 3.3) and formation of charged atomic species. For atomic oxygen, considering its high reactivity and lacking need of dissociation, immediate charge transfer is assumed upon contact with the metal surface. The reaction follows to place exchange between metal and charged atomic oxygen and formation of the first oxide monolayer. After this first monolayer is formed, a certain coverage of charged species should still exist on the surface for maintenance of V_M and continuation of oxide growth (one should be aware that, by then, the presence of oxide might influence the interaction between the surface and the charged species). As a simple analogy, the CM oxidation system can be viewed as a parallel-plate capacitor [32,66]. In a capacitor, however, the applied voltage determines the charge accumulated on the plates, while in the CM oxidation model the amount of adsorbed atomic oxygen determines the charge concentration and consequent electric field.

The influence of reactive atomic species on the value of formed V_M is directly evidenced by the differences in V_M between atomic- and molecular-oxygen exposed metals. Previous studies have shown that atomic oxygen presents a higher sticking probability than molecular oxygen on both pristine metal and oxidized surfaces for the analyzed metals [44,54,63,67–69]. Another point to be taken into account is that the probability of dissociative chemisorption of molecular oxygen decreases with increase of oxygen coverage [70]. With that, the probability of the existence (and maintenance) of a high atomic oxygen coverage and consequent surface charge density is superior upon direct atomic exposure. As previously mentioned, studies have suggested a dependence of Mott potential on the oxygen coverage based on variation of temperature and/or pressure [30,31,33,34]. The increase of V_M with coverage is further supported by analysis where processes such as ultraviolet [43,71] or electron [72] irradiation were employed during O_2 exposure. In these studies, an increase in final oxide thickness (compared to

pure O_2 exposure) was reported, strongly indicating that the presence of processes that induce O_2 dissociation (and consequent atomic oxygen surface concentration) lead to higher surface potential values.

Finally, looking specifically into atomic oxygen exposure, we can correlate the values of V_M to metal properties. According to the CM theory, the Mott potential is defined as $V_M = e^{-1}(\phi_0 - \phi_L)$ [7], with ϕ_0 the metal work function and ϕ_L the difference between the vacuum potential and the Fermi level in the presence of adsorbed oxygen. It is important to emphasize that this calculation of V_M is valid in the limit where the electron transmission from metal to adsorbed oxygen is dominated by the tunneling effect and cation diffusion is the limiting step in oxide formation [29]. With that, the lower the metal work function, the more negative the formed potential will be, and consequently the higher the generated field. Work function values for polycrystalline structures obtained from the literature show the lowest values for Hf (~4.0 eV) and Ta (~4.0 eV), followed by Mo (~4.3 eV) and Ru (~4.7 eV) [73]. One should be aware that the work function values are strongly dependent on surface properties, such as preferential plane and cleanliness. Therefore, values of work function reported in the literature often cover a considerable range. However, it is generally possible to correlate a lower work function to a more negative value of potential and consequently larger final oxide thickness for exposure of metals to atomic oxygen. As discussed, this is not necessarily true for molecular-oxygen exposures, where surface effects such as the competition between desorption and adsorption, together with coverage limitations directly influence the value of the Mott potential. As an example, based only on electronic characteristics, it was expected that Ru, among the analyzed metals, would present the lowest oxide formation for both molecular- and atomic-oxygen exposure. However, Mo and Ta formed thinner oxide than Ru for molecular-oxygen exposures in the analyzed T range. This difference can be related to the differences in catalytic ability of the initially formed oxide, as RuO_2 presents higher probability of O_2 dissociative chemisorption [68,74], leading to the maintenance of chemisorbed O concentration and consequent thicker oxide formation. These observations indicate that in cases where the presence of atomic oxygen species on the surface is not hindered by desorption or limited by coverage, the formed Mott field and the consequent limiting oxide thickness for low temperature oxidation can be directly related to the metal electronic properties.

3.4.2. Continuous oxide growth and crystalline oxide formation

Lastly, we should discuss the exposure conditions that do not present a self-limiting oxide growth: Hf at 473 K for both species; Ta at 473 K for O_2 , and from 423 K and 473 K for O; and Mo at 473 K for O_2 , and from 373 K to 473 K for O; Ru at 473 K for O. We hypothesize that at these conditions, three identified processes could potentially influence the maintenance of a continuous oxide growth within the timescale of the experiment: (i) increase in molecular dissociation (for molecular-

oxygen exposures); (ii) increase of ionic diffusion; (iii) contribution of electron transport by thermionic emission.

For molecular-oxygen exposure of Hf, Ta and Mo at 473 K, a rapid initial oxide growth followed by a decrease in rate with increasing exposure time is observed. However, this second oxidation stage is continuous, and the setting of growth in a limiting oxide thickness is not observed. This transition is observed for Hf, Ta and Mo at very thin oxide thicknesses, of about 0.7 nm, 0.6 nm and 0.2 nm respectively. This continuous growth could be induced by the increase of both molecular dissociation and ionic diffusion with temperature (with thermal diffusion induced by concentration gradients significant compared to field assisted oxide growth). As molecular-oxygen dissociation and the chemical diffusion of metal cations are thermally activated processes, the increase in temperature could enhance both the concentration of atomic oxygen species at the metal surface and number of cations diffusing for oxide formation. Both processes acting together can lead to a continuous supply of oxygen and cations for oxide formation, resulting in a continuous oxide growth. However, the slow rate of the second oxidation stage and the fact that the oxide thicknesses for all cases are still much lower than those obtained by direct atomic oxygen exposure indicate that surface processes might still be a limiting factor in the oxide growth dynamics.

For Ta at 423 K and 473 K, and Mo from 373 K to 473 K exposed to atomic species, an almost linear oxide growth is set, without observing a limiting oxide thickness. For both materials, the initial growth rate also decreases with increase of T . As discussed in the previous section, we propose that in these cases, the increase of temperature leads to a higher ionic diffusion through the oxide and consequent reduction of atomic oxygen coverage (i.e. rapid consumption of the O). A similar phenomenon has been recently observed for Cu oxidation at low temperatures [12]. As discussed by Unutulmazsoy *et al.* [12] for Cu, the different oxidation kinetics for Ta and Mo can be attributed to the very fast diffusion of cations in the corresponding oxides, which is comparably higher than typically observed for binary oxides. Usually in the low T regime, molecular dissociation seems to be a critical factor for further metal-oxygen reaction and oxide growth. However, direct exposure to atomic oxygen enables a direct oxide formation and high consumption of oxygen from the surface, which is accentuated with ion diffusion induced by further T increase. For Mo, the increase in ionic diffusion is supported by the stabilization of different oxidation states with temperature increase, observed in the XPS analysis. For Ta, such difference in oxidation states is likely not observed due to the higher reactivity of tantalum as compared with molybdenum [75].

This decrease in rate observed for Mo and Ta, however, is not observed for Ru and Hf exposed to atomic oxygen at 473 K. For these materials, a higher growth rate is observed during the entire oxidation. Both systems present a rapid initial oxide growth followed by a decrease in rate with increasing exposure time. However, Hf shows a significantly higher growth rate during the second stage compared to Ru, reaching a much thicker oxide than observed for the other metals after 300 min exposure. We hypothesize that the continuous growth observed for Ru and Hf at this exposure condition is a consequence of the increase of thermionic emission of electrons with T . Thermionic emission is a process considered to be strongly dependent on both metal properties and temperatures to which the system is exposed [28,76]. Considering the electronic properties of Hf, Ru and their oxides, and the analyzed temperature range, the effect of thermionic emission is negligible up to an oxide thickness of ~ 2 -3 nm, and the tunnel current is dominant in the charge transfer processes during oxide growth [27,28,76]. However, for thicknesses above this value and at a significant temperature, the tunnel current will cease and thermionic emission becomes the main charge transfer process. It is important to note that, contrary to tunneling, thermionic emission is independent of oxide thickness [28,32,76]. Therefore, even after the oxide reaches a thickness where the contribution of tunneling is reduced, electron transport through the thickening film remains. Following the constraint of coupled currents between

cations and electrons, the initial fast growth must be followed by a second stage of relatively slower, continuous oxide formation [29]. This transition between first fast and second slower stages is marked by a distinct drop in rate, a result of the breakdown of V_M by termination of tunneling. For Hf at 473 K, this transition is observed at ~ 2 nm oxide. This relative ease of electron transmission at 473 K and consequent oxide growth might be related to the lower work function of Hf and the high number of traps present in metal oxide films synthesized at lower temperatures, a phenomenon reported to be especially significant for HfO₂ thin films [77-79]. Considering the higher work function of Ru, the thermionic release of electrons should be less intense and, therefore, the oxide growth not as steep as observed for Hf. We hypothesize that the influence of thermionic emission would also be present for the other oxides that show continuous oxide growth at 473 K, however, the previously cited effects (increase in molecular dissociation and ionic diffusion) might be more determining for the growth in the other oxidation systems.

The final point to be discussed is the formation of crystalline oxides at 473 K for Hf, Ta and Mo exposed to atomic oxygen. Previous studies have demonstrated that for the oxide overgrowth on its metal substrate an amorphous phase is stable only up to a certain critical thickness [80,81]. The theoretical analysis developed by Reichel *et al.* [80] has demonstrated that this transition thickness is dependent on thermodynamical properties (such as bulk Gibbs energies, surface and interfacial energies) of both the metal and overgrown oxide films, and was estimated to lay in the range of ~ 1 -3 nm for oxides growing on densely packed monocrystalline metal surfaces. Therefore, the high reactivity and continuous oxide formation (induced by the phenomena discussed above) prompt the oxide growth past the thickness limit where the amorphous oxide overlayer is thermodynamically stable. However, we believe that temperature also plays a critical role in this phenomenon. This assumption is based on the observation that, even though Mo exposed to atomic O at 423 K and 473 K presents a similar final oxide thickness, only the sample exposed to the higher temperature shows the formation of crystalline oxide. For lower temperatures there may thus be a kinetic barrier that prevents formation of the more stable crystalline oxide phase. This interrelation between exposure conditions and crystalline oxide formation is an interesting phenomenon that will be further investigated in a future publication. However, preliminary experiments done in our research group have demonstrated that for HfO₂ growing on polycrystalline Hf, the crystallization of the oxide occurs at a thickness of approximately 5.5 nm. Furthermore, we observed that even after reaching of crystallization at 473 K, the oxide growth can be ceased by reducing the exposure temperature. This verification was done under a constant flow of atomic oxygen species and is a strong indication that, contrary to what was previously assumed [32], the oxide structure might not be the main factor leading to continuous oxide growth at low temperatures.

4. Key oxide formation characteristics for the analyzed metals

4.1. Hf

Hf samples present significant oxide formation for both molecular- and atomic-oxygen exposures, following a CM-type growth at $T \leq 423$ K for both species. No direct evidence of temperature influence on the V_M was observed, with values of -0.8 ± 0.2 V for molecular-oxygen exposure and -5.3 ± 0.3 V for atomic oxygen exposure. This difference indicates a significant effect of reactive species coverage on potential formation and consequent oxide growth. At $T = 473$ K, atomic oxygen interaction led to increased continuous oxide growth rate, forming a crystalline HfO₂ layer of ~ 15 nm after 300 min exposure. We hypothesize that this intense oxide growth is due to the transition of a tunneling mediated electron transfer to thermionic emission, a phenomenon marked by a distinct drop in growth rate between first fast and second slower growth stages at ~ 2 .0 nm oxide. This relative facility of electron transmission

is associated to the low work function of Hf and higher probability of electron trap formation for HfO₂ synthesized at lower temperatures.

4.2. Ta

Ta films present a CM-type growth at $T \leq 423$ K for O₂ and $T \leq 373$ K for O exposures. The significance of coverage for oxide formation was manifested in two different ways: for molecular oxygen, this was evidenced by the formation of a low V_M (-0.6 ± 0.1 V); for atomic oxygen, by the decrease of V_M with increased temperature. The first is associated to the lower molecular dissociation at the formed Ta₂O₅ surface, while the second is related to the increase in ion diffusion induced by T increase. The increase in ion diffusion is indicated by the almost linear rate of oxide growth. With intense oxide growth, at 473 K its thickness surpasses the limit in which amorphous oxide is thermodynamically stable and, therefore, a crystalline oxide structure is formed.

4.3. Mo

Mo presents significant oxide formation only for molecular-oxygen exposures at 473 K and direct atomic oxygen exposures. For molecular-oxygen exposures, the formation of a MoO₂ monolayer hinders further formation of oxide. The low reactivity of MoO₂ decreases the molecular dissociation probability, which impedes building up a significant V_M . As a result, only an increase of temperature to 473 K provides enough input of energy for continuous dissociation and oxide growth. For atomic oxygen exposures, the impediment of the oxidation reaction is no longer present, and oxide growth follows according to the CM mechanism up to 323 K. For higher temperatures, as in the case of Ta, the increase in ionic diffusion leads to a continuous oxide formation. Even though a similar oxide thickness is achieved for 423 K and 473 K, only the last temperature shows crystalline oxide formation (monoclinic Mo), indicating the critical influence of temperature in the structure stabilization of the formed oxide.

4.4. Ru

Upon both molecular- and atomic-oxygen exposure at temperatures below and equal than 473 K and 423 K respectively, Ru follows a field-driven oxide growth mechanism. The critical feature determining the maximum oxide thickness observed for this metal is the coverage of reactive atomic oxygen species. For molecular-oxygen exposures, at $T < 323$ K, the kinetic competition between oxygen desorption and dissociation at the Ru surface leads to an increase in desorption with increasing temperature. Consequently, below 323 K, there is an inverse relation between temperature and V_M . The exposure to atomic oxygen (and consequent higher coverage of reactive species) leads to values of V_M almost five times higher than for molecular-oxygen exposures (-2.9 ± 0.2 V for O exposure; -0.6 ± 0.1 V for O₂ exposure), resulting in faster oxide growth rates and formation of thicker oxide overlayers for all analyzed temperatures. For exposure to atomic oxygen at 473 K, we propose that the effect of thermionic emission induces the continuous oxide growth. However, at a lower rate than observed for Hf, considering the higher work function of Ru.

5. Conclusion

In this work the complete process of oxidation (from surface processes to film growth) was analyzed and described for polycrystalline Hf, Ta, Mo and Ru films. The reactions were studied at low temperatures (298 K to 473 K) upon the exposure to molecular oxygen and atomic oxygen.

Upon exposure to molecular oxygen, the surface O coverage rapidly saturates due to dissociative chemisorption. We observed that the initial growth rate up to an oxide thickness of ~ 0.3 nm can be described by an Arrhenius relation and we thus extracted the effective energy barriers

for molecular dissociation and penetration of oxygen to the sub-surface layer. Small differences in dissociation barrier were found compared to typical differences obtained for the dissociation energies of O₂ on clean metals. However, the effective energy barrier still scaled in the order from more to less reactive metals as Hf < Ta < Mo < Ru.

Considering the formation of oxide films beyond monolayer thickness, temperature limits for which Cabrera-Mott type growth is followed and the influence of oxidation specie on the formed potential and oxide growth dynamics were evaluated. A key finding from our studies was the demonstration that the surface concentration of reactive atomic species is the determining factor in the oxidation process for all analyzed metals. For the conditions that followed Cabrera-Mott type growth, all formed oxides were amorphous. The calculated values of energy barrier of diffusion were similar for both molecular- and atomic-oxygen exposures, indicating a similar atomic structure in the formed amorphous oxide films among the analyzed temperatures. For molecular-oxygen exposures, surface effects such as the competition between desorption and adsorption, together with coverage limitations directly influence the formed Mott potential (V_M) for $T < 473$ K. For atomic oxygen exposures, the high sticking and absence of a surface coverage limitation enable the correlation of lower work function (WF) to more negative values of the potential and consequently larger final oxide thickness, as determined by the Cabrera-Mott (CM) oxidation mechanism. The higher coverage derived upon O exposure was evident by the difference in potential and final oxide thickness formation. The values of V_M for O₂ exposure were higher than -1 V, with a small difference between the analyzed metals, while for atomic oxygen exposure the values scaled relative to WF decrease, from -2.9 eV (Ru) to -6.5 eV (Ta).

We also verified the interrelation between exposure conditions and crystalline oxide formation. Hf, Ta and Mo exposed to atomic oxygen at 473 K formed crystalline oxide structures, while Ru at the same exposure conditions remained amorphous. We hypothesize that the high reactivity and continuous oxide formation induced by increased ionic diffusion (Mo and Ta) and thermionic emission (Hf) prompt the oxide growth past the thickness limit where the amorphous oxide overlayer is thermodynamically stable. Nevertheless, temperature also has shown to present a critical role in oxide crystallization, as Mo exposed to atomic O at 423 K and 473 K present similar final oxide thickness, and only the sample exposed to the higher temperature showed the formation of crystalline oxide.

In the present study, the stages of oxide growth induced by molecular and atomic oxygen are analyzed thoroughly, and differences in final oxide composition and structure induced by the presence of activated oxygen species at low temperatures are covered. The obtained results provide a general guideline for synthesis and control of oxide growth on polycrystalline transition metal oxide thin films at low temperatures. The overall picture shows that in cases where the presence of atomic oxygen species on the surface is not hindered by desorption or limited by coverage, the formed Mott field, and consequently obtained limiting oxide thickness, at low temperature oxidation can be directly related to the metal electronic properties. We further hypothesize that this principle can be extended to other acceptor-type adsorbents, such as nitrogen: if radical species are directly in contact with the metal layer and enough coverage is present, a field assisted diffusion and compound growth process will be established. These results might have a significant impact, not only in the design of materials for a wide range of practical applications, but also for development of processes where reactive species are put in direct contact with thin layers (e.g. atomic layer growth or etching).

Declaration of Competing Interest

The authors declare that they have no known competing financial interests or personal relationships that could have appeared to influence the work reported in this paper.

Acknowledgements

This work is part of HTSM project 13913, funded by NWO Applied and Engineering Sciences with co-funding by Carl Zeiss SMT. The authors also acknowledge the Industrial Focus Group XUV Optics at the MESA+ Institute at the University of Twente, as well as the Province of Overijssel.

Supplementary materials

Supplementary material associated with this article can be found, in the online version, at [doi:10.1016/j.mta.2021.101203](https://doi.org/10.1016/j.mta.2021.101203).

References

- [1] M. Aykol, K.A. Persson, Oxidation Protection with Amorphous Surface Oxides: Thermodynamic Insights from Ab Initio Simulations on Aluminum, *ACS Appl. Mater. Interfaces*. 10 (2018) 3039–3045, doi:[10.1021/acsmi.7b14868](https://doi.org/10.1021/acsmi.7b14868).
- [2] V.P. Parkhutik, Modelling of low-temperature oxidation of materials in gaseous environments, *J. Phys. D: Appl. Phys.* 25 (1992) 256–261, doi:[10.1088/0022-3727/25/2/019](https://doi.org/10.1088/0022-3727/25/2/019).
- [3] P. Waldner, Modelling of oxygen solubility in titanium, *Scr. Mater.* 40 (1999) 969–974, doi:[10.1016/S1359-6462\(99\)00053-6](https://doi.org/10.1016/S1359-6462(99)00053-6).
- [4] H.A. Baroody, G. Jerkiewicz, M.H. Eikerling, Modelling oxide formation and growth on platinum, *J. Chem. Phys.* (2017) 146, doi:[10.1063/1.4979121](https://doi.org/10.1063/1.4979121).
- [5] J. Gustafson, A. Mikkelsen, M. Borg, E. Lundgren, L. Köhler, G. Kresse, M. Schmid, P. Varga, J. Yuhara, X. Torrelles, C. Quirós, J.N. Andersen, Self-limited growth of a thin oxide layer on Rh(111), *Phys. Rev. Lett.* 92 (2004) 10–13, doi:[10.1103/PhysRevLett.92.126102](https://doi.org/10.1103/PhysRevLett.92.126102).
- [6] I. Nishiyama, Model of Ru surface oxidation for the lifetime scaling of EUVL projection optics mirror, in: *Proc. SPIE*, 2006, p. 6151, doi:[10.1117/12.655499](https://doi.org/10.1117/12.655499).
- [7] N. Cabrera, N.F. Mott, Theory of the oxidation of metals, *Rep. Prog. Phys.* 12 (1949) 163–184 <https://doi.org/10.1034/4885/12/1/308>.
- [8] G. Bakradze, L.P.H. Jeurgens, E.J. Mittemeijer, Oxide-film growth kinetics on Zr(0001) and Zr(1010) single-crystal surfaces, *Surf. Interface Anal.* 42 (2010) 588–591, doi:[10.1002/sia.3235](https://doi.org/10.1002/sia.3235).
- [9] E.H. Voogt, A.J.M. Mens, O.L.J. Gijzeman, J.W. Geus, Adsorption of oxygen and surface oxide formation on Pd(111) and Pd foil studied with ellipsometry, LEED, AES and XPS, *Surf. Sci.* 373 (1997) 210–220, doi:[10.1016/S0039-6028\(96\)01180-6](https://doi.org/10.1016/S0039-6028(96)01180-6).
- [10] K. Radican, N. Berdunov, G. Manai, I.V. Shvets, Epitaxial molybdenum oxide grown on Mo(110): LEED, STM, and density functional theory calculations, *Phys. Rev. B - Condens. Matter Mater. Phys.* 75 (2007) 1–7, doi:[10.1103/PhysRevB.75.155434](https://doi.org/10.1103/PhysRevB.75.155434).
- [11] C.R. Stilhano Vilas Boas, J.M. Sturm, F. Bijkerk, Oxidation of metal thin films by atomic oxygen: A low energy ion scattering study, *J. Appl. Phys.* 126 (2019) 155301, doi:[10.1063/1.5115112](https://doi.org/10.1063/1.5115112).
- [12] Y. Unutulmazsoy, C. Cancellieri, M. Chiodi, S. Siol, L. Lin, L.P.H. Jeurgens, In situ oxidation studies of Cu thin films: Growth kinetics and oxide phase evolution, *J. Appl. Phys.* (2020) 127, doi:[10.1063/1.5131516](https://doi.org/10.1063/1.5131516).
- [13] Y. Sasaki, M. Kawamura, T. Kiba, Y. Abe, K.H. Kim, H. Murotani, Improved durability of Ag thin films under high humidity environment by deposition of surface Al nanolayer, *Appl. Surf. Sci.* 506 (2020) 144929, doi:[10.1016/j.apsusc.2019.144929](https://doi.org/10.1016/j.apsusc.2019.144929).
- [14] A. Seyeux, V. Maurice, P. Marcus, Oxide Film Growth Kinetics on Metals and Alloys: I. Physical Model, *J. Electrochem. Soc.* 160 (2013) C189–C196, doi:[10.1149/2.036306jes](https://doi.org/10.1149/2.036306jes).
- [15] R.E. Smallman, R.J. Bishop, *Modern Physical Metallurgy and Materials Engineering*, Mod. Phys. Metall. Mater. Eng. (1999) 320–350, doi:[10.1016/B978-075064564-5/50010-0](https://doi.org/10.1016/B978-075064564-5/50010-0).
- [16] H. Mehrer, *Diffusion in solids: fundamentals, methods, materials, diffusion-controlled processes*, Springer, 2007, doi:[10.1007/978-3-540-71488-0](https://doi.org/10.1007/978-3-540-71488-0).
- [17] N. Birks, G.H. Meier, F.S. Pettit, *Introduction to the high temperature oxidation of metals*, Second edition, Cambridge University Press, 2006, doi:[10.1017/CBO9781139163903](https://doi.org/10.1017/CBO9781139163903).
- [18] L.P.H. Jeurgens, A. Lyapin, E.J. Mittemeijer, The mechanism of low-temperature oxidation of zirconium, *Acta Mater* 53 (2005) 4871–4879, doi:[10.1016/j.actamat.2005.06.028](https://doi.org/10.1016/j.actamat.2005.06.028).
- [19] U. Khalilov, A. Bogaerts, E.C. Neyts, Toward the Understanding of Selective Si Nano-Oxidation by Atomic Scale Simulations, *Acc. Chem. Res.* 50 (2017) 796–804, doi:[10.1021/acs.accounts.6b00564](https://doi.org/10.1021/acs.accounts.6b00564).
- [20] C.R. Stilhano Vilas Boas, A.A. Zameshin, J.M. Sturm, F. Bijkerk, The influence of oxygen on the neutralization of slow helium ions scattered from transition metals and aluminum surfaces, *Surf. Sci.* 700 (2020) 121680, doi:[10.1016/j.susc.2020.121680](https://doi.org/10.1016/j.susc.2020.121680).
- [21] P. Phadke, C.R. Stilhano Vilas Boas, J.M. Sturm, R.W.E. van de Kruijs, F. Bijkerk, Near-threshold, steady state interaction of oxygen ions with transition metals: Sputtering and radiation enhanced diffusion, *Appl. Surf. Sci.* 518 (2020) 146143 <https://doi.org/10.1016/j.apsusc.2020.146143>.
- [22] R. Franchy, Growth of thin, crystalline oxide, nitride and oxynitride films on metal and metal alloy surfaces, *Surf. Sci. Rep.* 38 (2000) 195–294 [https://doi.org/http://dx.doi.org/10.1016/S0167-5729\(99\)00013-8](https://doi.org/http://dx.doi.org/10.1016/S0167-5729(99)00013-8).
- [23] S. Bajt, N.V. Edwards, T.E. Madey, Properties of ultrathin films appropriate for optics capping layers exposed to high energy photon irradiation, *Surf. Sci. Rep.* 63 (2008) 73–99, doi:[10.1016/j.surfrep.2007.09.001](https://doi.org/10.1016/j.surfrep.2007.09.001).
- [24] M.T. Greiner, L. Chai, M.G. Helander, W.M. Tang, Z.H. Lu, Transition metal oxide work functions: The influence of cation oxidation state and oxygen vacancies, *Adv. Funct. Mater.* 22 (2012) 4557–4568, doi:[10.1002/adfm.201200615](https://doi.org/10.1002/adfm.201200615).
- [25] C.T. Campbell, Ultrathin metal films and particles on oxide surfaces: structural, electronic and chemisorption properties, *Surf. Sci. Rep.* 27 (1997) 1–111, doi:[10.1016/S0167-5729\(96\)00011-8](https://doi.org/10.1016/S0167-5729(96)00011-8).
- [26] Q. Fu, T. Wagner, Interaction of nanostructured metal overlayers with oxide surfaces, *Surf. Sci. Rep.* 62 (2007) 431–498, doi:[10.1016/j.surfrep.2007.07.001](https://doi.org/10.1016/j.surfrep.2007.07.001).
- [27] A.T. Fromhold, E.L. Cook, Kinetics of oxide film growth on metal crystals: Electron tunneling and ionic diffusion, *Phys. Rev.* 158 (1967) 600–612, doi:[10.1103/PhysRev.158.600](https://doi.org/10.1103/PhysRev.158.600).
- [28] A.T. Fromhold, E.L. Cook, Kinetics of oxide film growth on metal crystals: Thermal electron emission and ionic diffusion, *Phys. Rev.* 163 (1967) 650–664, doi:[10.1103/PhysRev.163.650](https://doi.org/10.1103/PhysRev.163.650).
- [29] A.T. Fromhold, *Theory of Metal Oxidation*, North Holland Publishing Company, Amsterdam, 1976.
- [30] N. Cai, G. Zhou, K. Müller, D.E. Starr, Temperature and pressure dependent Mott potentials and their influence on self-limiting oxide film growth, *Appl. Phys. Lett.* 101 (2012) 1–5, doi:[10.1063/1.4764552](https://doi.org/10.1063/1.4764552).
- [31] N. Cai, G. Zhou, K. Müller, D.E. Starr, Effect of oxygen gas pressure on the kinetics of alumina film growth during the oxidation of Al(111) at room temperature, *Phys. Rev. B - Condens. Matter Mater. Phys.* 84 (2011) 1–6, doi:[10.1103/PhysRevB.84.125445](https://doi.org/10.1103/PhysRevB.84.125445).
- [32] L.P.H. Jeurgens, W.G. Sloof, F.D. Tichelaar, E.J. Mittemeijer, Growth kinetics and mechanisms of aluminum-oxide films formed by thermal oxidation of aluminum, *J. Appl. Phys.* 92 (2002) 1649–1656, doi:[10.1063/1.1491591](https://doi.org/10.1063/1.1491591).
- [33] A. Lyapin, L.P.H. Jeurgens, E.J. Mittemeijer, Effect of temperature on the initial, thermal oxidation of zirconium, *Acta Mater* 53 (2005) 2925–2935, doi:[10.1016/j.actamat.2005.03.009](https://doi.org/10.1016/j.actamat.2005.03.009).
- [34] S.K.R.S. Sankaranarayanan, S. Ramanathan, On the Low-Temperature Oxidation and Ultrathin Oxide Growth on Zirconium in the Presence of Atomic Oxygen: A Modeling Study, *J. Phys. Chem. C* 112 (2008) 17877–17882 <https://doi.org/10.1021/jp804872u>.
- [35] J.H. Scofield, Hartree-Slater subshell photoionization cross-sections at 1254 and 1487 eV, *J. Electron Spectrosc. Relat. Phenomena* 8 (1976) 129–137, doi:[10.1016/0368-2048\(76\)80015-1](https://doi.org/10.1016/0368-2048(76)80015-1).
- [36] M. Khanuja, H. Sharma, B.R. Mehta, S.M. Shivaprasad, XPS depth-profile of the sub-oxide distribution at the native oxide/Ta interface, *J. Electron Spectrosc. Relat. Phenomena* 169 (2009) 41–45, doi:[10.1016/j.elspec.2008.10.004](https://doi.org/10.1016/j.elspec.2008.10.004).
- [37] C. Morant, L. Galán, J.M. Sanz, An XPS study of the initial stages of oxidation of hafnium, *Surf. Interface Anal.* 16 (1990) 304–308, doi:[10.1002/sia.740160163](https://doi.org/10.1002/sia.740160163).
- [38] S. Guimond, J.M. Sturm, D. Göbke, Y. Romanyshyn, M. Naschitzki, H. Kühlenbeck, H.J. Freund, Well-ordered v2O5(001) thin films on Au(111): Growth and thermal stability, *J. Phys. Chem. C* 112 (2008) 11835–11846, doi:[10.1021/jp8011156](https://doi.org/10.1021/jp8011156).
- [39] M.N. Polyanskiy, Refractive index database, (n.d.). <https://refractiveindex.info> (accessed October 19, 2020).
- [40] A. Lyapin, L.P.H. Jeurgens, P.C.J. Graat, E.J. Mittemeijer, Ellipsometric and XPS study of the initial oxidation of zirconium at room temperature, *Surf. Interface Anal.* 36 (2004) 989–992, doi:[10.1002/sia.1819](https://doi.org/10.1002/sia.1819).
- [41] S. Guimond, D. Göbke, J.M. Sturm, Y. Romanyshyn, H. Kühlenbeck, M. Cavalleri, H.J. Freund, Well-ordered molybdenum oxide layers on Au(111): Preparation and properties, *J. Phys. Chem. C* 117 (2013) 8746–8757, doi:[10.1021/jp3113792](https://doi.org/10.1021/jp3113792).
- [42] L. Nguyen, T. Hashimoto, D.N. Zakharov, E.A. Stach, A.P. Rooney, B. Berkels, G.E. Thompson, S.J. Haigh, T.L. Burnett, P. Aidan, B. Berkels, Atomic-Scale Insights into the Oxidation of Aluminum, *ACS Appl. Mater. Interfaces*. 10 (2018) 2230–2235, doi:[10.1021/acsmi.7b17224](https://doi.org/10.1021/acsmi.7b17224).
- [43] S. Ramanathan, D. Chi, P.C. McIntyre, C.J. Wetteland, J.R. Tesmer, Ultraviolet-Ozone Oxidation of Metal Films, *J. Electrochem. Soc.* 150 (2003) F110, doi:[10.1149/1.1566416](https://doi.org/10.1149/1.1566416).
- [44] K. Reuter, C. Stampfl, M. Verónica Ganduglia-Pirovano, M. Scheffler, Atomistic description of oxide formation on metal surfaces: The example of ruthenium, *Chem. Phys. Lett.* 352 (2002) 311–317, doi:[10.1016/S0009-2614\(01\)01472-5](https://doi.org/10.1016/S0009-2614(01)01472-5).
- [45] M.A. Ernst, W.G. Sloof, Unraveling the oxidation of Ru using XPS, *Surf. Interface Anal.* (2008) 334–337, doi:[10.1002/sia.2675](https://doi.org/10.1002/sia.2675).
- [46] M. Birkholz, *Thin Film Analysis by X-ray*, WILEY-VCH Verlag GmbH & Co, KGaA, Weinheim (2006), doi:[10.1002/3527607595](https://doi.org/10.1002/3527607595).
- [47] A. Needleman, S. Suresh (Eds.), *Stress and grain Growth in thin films*, *J Mech Phys Solids* (1996) [https://doi.org/10.1016/S0022-5096\(96\)00022-1](https://doi.org/10.1016/S0022-5096(96)00022-1).
- [48] R.C. Ribera, R.W.E. Van De Kruijs, S. Kokke, E. Zoethout, A.E. Yakshin, F. Bijkerk, Surface and sub-surface thermal oxidation of thin ruthenium films, *Appl. Phys. Lett.* 105 (2014) 13–18, doi:[10.1063/1.4896993](https://doi.org/10.1063/1.4896993).
- [49] C.V. Ramana, K.Kamala Bharathi, A. Garcia, A.L. Campbell, Growth behavior, lattice expansion, strain, and surface morphology of nanocrystalline, monoclinic HfO₂ thin films, *J. Phys. Chem. C* 116 (2012) 26681–26682, doi:[10.1021/jp310937u](https://doi.org/10.1021/jp310937u).
- [50] K. Kukli, J. Ihanus, M. Ritala, M. Leskela, Tailoring the dielectric properties of HfO₂-Ta₂O₅ nanolaminates, *Appl. Phys. Lett.* 68 (1996) 648–657, doi:[10.31857/s0044457x21050202](https://doi.org/10.31857/s0044457x21050202).
- [51] C.R. Stilhano Vilas Boas, J.M. Sturm, I. Milov, P. Phadke, F. Bijkerk, Room temperature oxygen exchange and diffusion in nanometer-thick ZrO₂ and MoO₃ films, *Appl. Surf. Sci.* 550 (2021) 1–9, doi:[10.1016/j.apsusc.2021.149384](https://doi.org/10.1016/j.apsusc.2021.149384).
- [52] K.R. Lawless, The oxidation of metals, *Rep. Prog. Phys.* 37 (1974) 231–316 <https://doi.org/10.1088/0034-4885/37/2/002>.
- [53] E.D. German, M. Sheintuch, Relationship between kinetic and thermodynamic characteristics of oxygen dissociative adsorption on close-packed metal surfaces, *J. Phys. Chem. A* 109 (2005) 7957–7966, doi:[10.1021/jp051678+](https://doi.org/10.1021/jp051678+).
- [54] M.C. Wheeler, D.C. Seets, C.B. Mullins, Kinetics and dynamics of the initial dissociative chemisorption of oxygen on Ru(001), *J. Chem. Phys.* 105 (1996) 1572–1583, doi:[10.1063/1.472018](https://doi.org/10.1063/1.472018).

- [55] P.D. Nolan, M.C. Wheeler, J.E. Davis, C.B. Mullins, Mechanisms of Initial Dissociative Chemisorption of Oxygen on Transition-Metal Surfaces, *Acc. Chem. Res.* 31 (1998) 798–804, doi:10.1021/ar960278p.
- [56] B.A. Ferguson, C.T. Reeves, C.B. Mullins, Oxygen adsorption on Si(100)-2x1 via trapping-mediated and direct mechanisms, *J. Chem. Phys.* 110 (1999) 11574–11584, doi:10.1063/1.478005.
- [57] B. Bruckner, P. Bauer, D. Primetzhofer, Neutralization of slow helium ions scattered from single crystalline aluminum and tantalum surfaces and their oxides, *Surf. Sci.* 691 (2020) 121491, doi:10.1016/j.susc.2019.121491.
- [58] I. Kavre Piltaver, I. Jelovica Badovinac, R. Peter, I. Saric, M. Petracic, Modification of molybdenum surface by low-energy oxygen implantation at room temperature, *Appl. Surf. Sci.* 425 (2017) 416–422, doi:10.1016/j.apsusc.2017.07.029.
- [59] S.I. Castañeda, I. Montero, J.M. Ripalda, N. Díaz, L. Galán, F. Rueda, X-ray photoelectron spectroscopy study of low-temperature molybdenum oxidation process, *J. Appl. Phys.* 85 (1999) 8415–8418, doi:10.1063/1.370690.
- [60] E. Minni, F. Werfel, Oxygen interaction with Mo(100) studied by XPS, AES and EELS, *Surf. Interface Anal* 12 (1988) 385–390, doi:10.1002/sia.740120704.
- [61] T.B. Fryberger, P.C. Stair, The metal-oxide transition on Mo(100) monitored by photoemission of physisorbed xenon, *Chem. Phys. Lett.* 93 (1982) 151–156, doi:10.1016/0009-2614(82)83683-X.
- [62] P. Hofmann, K. Horn, A.M. Bradshaw, K. Jacobi, The adsorption and condensation of oxygen on aluminium at low temperature, *Surf. Sci.* 82 (1979) 610–614, doi:10.1016/0039-6028(79)90218-8.
- [63] M.M. Montemore, M.A. Van Spronsen, R.J. Madix, C.M. Friend, O₂ Activation by Metal Surfaces: Implications for Bonding and Reactivity on Heterogeneous Catalysts, *Chem. Rev.* 118 (2018) 2816–2862, doi:10.1021/acs.chemrev.7b00217.
- [64] A. Vojvodic, J.K. Nørskov, F. Abild-Pedersen, Electronic structure effects in transition metal surface chemistry, *Top. Catal.* 57 (2014) 25–32, doi:10.1007/s11244-013-0159-2.
- [65] G. Zhou, *Air-Formed Film: Mott–Cabrera Model*, Elsevier, 2017, doi:10.1016/b978-0-12-409547-2.13396-7.
- [66] D.J. Griffiths, *Introduction to Electrodynamics*, 3rd ed., Prentice-Hall, Inc, 1999, doi:10.1017/CBO9781107415324.004.
- [67] B. Herd, H. Over, Atomic scale insights into the initial oxidation of Ru(0001) using atomic oxygen, *Surf. Sci.* 622 (2014) 24–34, doi:10.1016/j.susc.2013.11.017.
- [68] Y.D. Kim, A.P. Seitsonen, S. Wendt, J. Wang, C. Fan, K. Jacobi, H. Over, G. Ertl, Characterization of various oxygen species on an oxide surface: RuO₂(110), *J. Phys. Chem. B.* 105 (2001) 3752–3758, doi:10.1021/jp003213j.
- [69] A.M. Horgan, D.A. King, Oxygen adsorption, reconstruction, and thin oxide film formation on clean metal surfaces: Ni, Fe, W and Mo, *Surf. Sci.* 23 (1970) 259–282.
- [70] F.P. Fehlner, N.F. Mott, Low-temperature oxidation, *Oxid. Met.* 2 (1970) 59–99, doi:10.1007/BF00603582.
- [71] M. Tsuchiya, S.K.R.S. Sankaranarayanan, S. Ramanathan, Photon-assisted oxidation and oxide thin film synthesis: A review, *Prog. Mater. Sci.* 54 (2009) 981–1057, doi:10.1016/j.pmatsci.2009.04.003.
- [72] V. Zhukov, I. Popova, J.T. Yates, Electron-stimulated oxidation of Al(111) by oxygen at low temperatures: Mechanism of enhanced oxidation kinetics, *Phys. Rev. B - Condens. Matter Mater. Phys.* 65 (2002) 1–6, doi:10.1103/PhysRevB.65.195409.
- [73] W.M. Haynes, *CRC Handbook of Chemistry and Physics*, 95th ed., CRC Press, 2014.
- [74] H. Over, Y.D. Kim, A.P. Seitsonen, S. Wendt, E. Lundgren, M. Schmid, P. Varga, A. Morgante, G. Ertl, Atomic-scale structure and catalytic reactivity of the RuO₂(110) surface, *Science* (80-.). 287 (2000) 1474–1476. https://doi.org/10.1126/science.287.5457.1474.
- [75] N.V. Alov, Surface oxidation of metals by oxygen ion bombardment, *Nucl. Instruments Methods Phys. Res. Sect. B Beam Interact. with Mater. Atoms.* 256 (2007) 337–340, doi:10.1016/j.nimb.2006.12.023.
- [76] E.L. Murphy, R.H. Good, Thermionic Emission, Field Emission, and the Transition Region, *Phys. Rev.* 102 (1956) 1464–1473, doi:10.1103/PhysRev.102.1464.
- [77] P.T. Liu, C.T. Tsai, P.Y. Yang, Effects of supercritical CO₂ fluid on sputter-deposited hafnium oxide, *Appl. Phys. Lett.* (2007) 90, doi:10.1063/1.2743747.
- [78] G.D. Wilk, R.M. Wallace, J.M. Anthony, High- κ gate dielectrics: Current status and materials properties considerations, *J. Appl. Phys.* 89 (2001) 5243–5275, doi:10.1063/1.1361065.
- [79] D. Brassard, D.K. Sarkar, M.A. El Khakani, L. Ouellet, Compositional effect on the dielectric properties of high- κ titanium silicate thin films deposited by means of a cosputtering process, *J. Vac. Sci. Technol. A Vacuum, Surfaces, Film* 24 (2006) 600–605, doi:10.1116/1.2180267.
- [80] F. Reichel, L.P.H. Jeurgens, E.J. Mittemeijer, The thermodynamic stability of amorphous oxide overgrowths on metals, *Acta Mater* 56 (2008) 659–674, doi:10.1016/j.actamat.2007.10.023.
- [81] F. Reichel, *The effect of substrate orientation on the kinetics and thermodynamics of initial oxide-film growth on metals*, University of Stuttgart, 2007.